

First Tellurite Composite Fiber with NIR-Driven Green Persistent Luminescence

Evellyn Santos Magalhães, Khaldoon Nasser, Arjun Vakkada Ramachandran, Mikko Närhi, Minnea Tuomisto, Catherine Boussard-Plédel, Johann Troles, Philippe F. Smet, Mika Lastusaari, and Laeticia Petit*

Expanding the excitation range of persistent luminescent (PeL) materials into the near infrared (NIR) region is critical to enable remote, flexible, and compact advanced optical systems. In this study, the fabrication of the first composite fiber based on $\text{SrAl}_2\text{O}_4:\text{Eu}^{2+}$, Dy^{3+} phosphors embedded in $\text{Yb}^{3+}/\text{Tm}^{3+}$ co-doped tellurite glass is reported. The fiber is drawn from a translucent, crack-free composite preform prepared with 0.5 wt.% PeL phosphors. Light propagation in the fiber is demonstrated despite the presence of the PeL phosphors. Long-lasting green emission from the preform and fiber is driven by 980 nm and suggests the survival of the PeL phosphors during the preform preparation and fiber drawing processes. The presence of the PeL phosphors in the glass matrix is confirmed using SEM/EDS composition analysis. This work offers a practical and scalable approach for integrating NIR-excitable PeL materials into fiber-based platforms, opening new opportunities for their application in advanced photonic technologies.

1. Introduction

Persistent luminescence (PeL), also known as afterglow, refers to the continued emission of light even after the excitation source has been removed. This effect occurs after absorbing high-energy radiation, such as X-rays, UV, or visible light, followed by trapping charge carriers (electrons or holes) in the crystal structure, either locally around the luminescent center or in defects over the lattice. These trapped carriers are then released by thermal energy, leading to sustained emission lasting for minutes or even hours.^[1–4]

Interest in the PeL phosphors arose in the 1990s, after the groundbreaking report on the long-lasting afterglow from $\text{SrAl}_2\text{O}_4:\text{Eu}^{2+}$, Dy^{3+} phosphors by Matsuzawa et al.^[5] Since then, the field has

expanded rapidly, with numerous studies reporting dozens of new PeL materials, such as $\text{Zn}_3\text{Ga}_2\text{GeO}_8:\text{Cr}^{3+}$,^[6] $\text{ZnGa}_2\text{O}_4:\text{Cr}^{3+}$,^[7] $\text{LiGa}_5\text{O}_8:\text{Cr}^{3+}$, $\text{MgGeO}_3:\text{Pr}^{3+}$, just to cite a few.^[8] Today, the PeL materials are used in diverse domains, including roadway markings, dye-sensitized solar cells, radiation dosimetry, and photocatalysis.^[9,10] Among the known PeL materials, the $\text{SrAl}_2\text{O}_4:\text{Eu}^{2+}$, Dy^{3+} phosphor is remarkable for its characteristic green emission and long decay time after UV charging.^[2,5] The mechanism of the afterglow in $\text{SrAl}_2\text{O}_4:\text{Eu}^{2+},\text{Dy}^{3+}$ involves a sequence of charge carrier excitation, trapping, and delayed recombination. Upon excitation with UV or short-wavelength visible photons, Eu^{2+} ions absorb energy and transition to an excited state. The Dy^{3+} ions act as trap centers, capturing electrons generated by the excitation of Eu^{2+} .^[11] After the excitation source is removed, ambient thermal energy slowly releases (detraps) electrons from these traps over time. The trap depth determines how quickly or slowly the carriers are released. Once released, the carriers recombine at the Eu^{2+} luminescent centers, resulting in the characteristic blue-green emission.^[12,13]

Fibers with PeL have emerged as promising tools for advanced biomedical imaging and health monitoring due to their ability to store and gradually release light energy. For example, bio-integrated PeL fibers provide non-invasive optical sensing and enable long-term tracking of cells, tissues, or drug delivery pathways.^[14–16] PeL fibers open new opportunities for

E. S. Magalhães, K. Nasser, A. V. Ramachandran, M. Närhi, L. Petit
Photonics Laboratory
Tampere University
Korkeakoulunkatu 3, Tampere 33720, Finland
E-mail: khaldoon.nasser@tuni.fi

C. Boussard-Plédel, J. Troles
Institut des Sciences Chimiques de Rennes
University Rennes
CNRS
263 Av. Général Leclerc, Rennes 35700, France

P. F. Smet
LumiLab
Department of Solid State Sciences
Ghent University
Krijgslaan 281-S1, Gent 9000, Belgium

M. Tuomisto, M. Lastusaari
Department of Chemistry
University of Turku
Turku 20014, Finland

 The ORCID identification number(s) for the author(s) of this article can be found under <https://doi.org/10.1002/adom.202502249>

© 2025 The Author(s). Advanced Optical Materials published by Wiley-VCH GmbH. This is an open access article under the terms of the [Creative Commons Attribution](#) License, which permits use, distribution and reproduction in any medium, provided the original work is properly cited.

DOI: 10.1002/adom.202502249

multifunctional textiles and security technologies.^[17,18] In anti-counterfeiting, they enable luminescent authentication patterns that can be woven directly into fabrics. These fibers can carry unique optical signatures or encrypted luminescent codes that become visible only under specific conditions, providing a reliable method for fraud prevention and secure identification.^[17,18]

There are different approaches to create PeL fibers. For example, $\text{SrAl}_2\text{O}_4:\text{Eu}^{2+}$, Dy^{3+} , $\text{Sr}_2\text{ZnSi}_2\text{O}_7:\text{Eu}^{2+}$, Dy^{3+} , and $\text{Y}_2\text{O}_2\text{S}:\text{Eu}^{3+}, \text{Mg}^{2+}, \text{Ti}^{4+}$ were synthesized and incorporated into luminous polymer fibers using the one-step extrusion wet-spinning process.^[19] Ge et al. examined microstructure, composition, and afterglow properties of luminescent fibers by using polyethylene terephthalate (PET) polymer as a matrix through a melt spinning process.^[20] $\text{SrAl}_2\text{O}_4:\text{Eu}^{2+}$, Dy^{3+} phosphors were also mixed with PET to produce luminescent fibers using a twin-screw extruder.^[21] Chen et al. experimented with the preparation of SrAl_2O_4 doped with 0.1% to 1.4% of Eu^{2+} and Dy^{3+} to analyze the effect on the luminescent effect of the fiber melt spinning process when incorporating into polyamide-6, which also exhibited persistent luminescence in the visible spectrum.^[22] Barbosa et al. incorporated $\text{Zn}_2\text{GeO}_4:\text{Mn}^{2+}$ into polyvinyl alcohol (PVA) fibers which showed green PeL.^[23] The above-mentioned polymer-based methods for fabricating PeL fibers are attractive due to their scalability and simplicity, but they come with significant drawbacks. High processing temperatures can degrade the temperature-sensitive phosphor, while poor dispersion may lead to phosphor agglomeration, causing uneven luminescence. Additionally, incorporating inorganic fillers often compromises the mechanical properties of the fibers. The well-known moisture sensitivity of the phosphors can further reduce the long-term stability of the fiber. These limitations suggest that alternative approaches should be developed, such as embedding phosphors in glass matrices which may offer superior luminescent and better structural performance. Lemiere et al. prepared preforms by remelting the bioactive glass with the composition $50\text{P}_2\text{O}_5-40\text{SrO}-10\text{Na}_2\text{O}$ (in mol%) with $\text{SrAl}_2\text{O}_4:\text{Eu}^{2+}$, Dy^{3+} PeL phosphors.^[14] These preforms were then drawn into fibers, resulting in composite fibers exhibiting green afterglow after UV charging. The duration of the remelt step was minimized to limit the decomposition of the PeL phosphors, and despite some changes in the site of Eu^{2+} occurring during drawing, the fibers exhibit green afterglow after UV charging.

Recent studies have investigated the potential of near-infrared (NIR) light (650–1000 nm) to charge the PeL phosphors, to broaden their applicability. Unlike ultraviolet (UV) light, NIR light penetrates more deeply into biological tissues, enabling advanced in vivo applications such as bioimaging, disease tracking, and therapeutic monitoring.^[14,15,24–26] A promising strategy involves incorporating upconversion ion pairs, such as Yb^{3+} , Tm^{3+} , alongside PeL phosphors.^[27–29] Cheap 980 nm commercially available laser diodes can be used to excite Yb^{3+} ions, due to their large absorption cross-section at this wavelength. The excitation energy can then be transferred to Tm^{3+} ions, which then emit UV/blue light through upconversion, leading to charging of the $\text{SrAl}_2\text{O}_4:\text{Eu}^{2+}$, Dy^{3+} PeL phosphors.^[24,27–30] While NIR chargeable PeL phosphors and bulk have been achieved,^[14,15,24–30] there have been no published studies to date demonstrating PeL fibers that can be charged using NIR light.

Selecting an appropriate glass matrix to host the PeL phosphors is essential to preserve the luminescence properties of the PeL phosphors and enable further processing, such as fiber drawing. An ideal host should possess a high refractive index to closely match that of the phosphor crystals (≈ 1.76) and the phosphors must be uniformly dispersed throughout the glass matrix without aggregation to guarantee the preparation of transparent composite fibers with minimized light scattering.^[31] Tellurite glasses are particularly well-suited to host PeL phosphors as they offer high refractive index (≈ 2.0). They also possess low phonon energy ($600-800\text{ cm}^{-1}$) and a broad transmission window ($0.38-6\text{ }\mu\text{m}$). Moreover, tellurite glasses exhibit high solubility for rare-earth (RE) ions, and relatively low melting temperatures when compared to silica glasses.^[32–34] These characteristics make them highly suitable for diverse applications, ranging from fiber amplifiers and supercontinuum generation to medical devices such as endoscopes.^[35–38] Tellurite glasses co-doped with Yb^{3+} and Tm^{3+} have become attractive for upconversion applications. Particularly, the tellurite glass with the composition $70\text{TeO}_2-20\text{ZnO}-10\text{BaO}$ (in mol%) has demonstrated great stability against crystallization, making them excellent candidates for fiber drawing.^[39–42]

Therefore, this work aims to develop and investigate PeL composite fibers by incorporating $\text{SrAl}_2\text{O}_4:\text{Eu}^{2+}, \text{Dy}^{3+}$ PeL phosphor into Yb^{3+} , Tm^{3+} co-doped tellurite glass, which is then drawn into a fiber. This Yb^{3+} and Tm^{3+} codoping approach enables the charging of the PeL material using NIR via upconversion process. In this study we explore this pathway for creating new NIR-rechargeable PeL fibers for possible applications in advanced biomedical imaging, for example.

2. Results and Discussion

Tellurite glasses, due to their low phonon energies, have been considered promising candidates for upconversion luminescence, especially the $70\text{TeO}_2-20\text{ZnO}-10\text{BaO}$ glass composition (in mol%).^[42]

As outlined in our previous work,^[29] the UV/blue emission must reach sufficient intensity to effectively charge the $\text{SrAl}_2\text{O}_4:\text{Eu}^{2+}$, Dy^{3+} PeL phosphor. Herein, the tellurite glasses were synthesized with varying concentrations of Yb_2O_3 (1.5–4.5 mol%) and Tm_2O_3 (0.025–0.1 mol%) in order to prepare a glass with strong UV/blue emission while ensuring thermal stability suitable for fiber drawing. **Table 1** shows the thermal and physical properties of some of the investigated glasses. When the concentration of Yb_2O_3 and Tm_2O_3 increases, the glass transition temperature (T_g), the onset of crystallization (T_x), and the crystallization temperatures (T_p) increase due to changes in the glass structure as evidenced by the Raman spectra shown in **Figure 1a**. An increase in RE content induces a slight depolymerization of the glass network, as evidenced by the enhanced intensity of the band at 745 cm^{-1} , attributed to $\text{TeO}_3/\text{TeO}_{3+1}$ structural units, relative to the band at 664 cm^{-1} , which corresponds to TeO_4 units.^[42] Elkhoshkhany et al. reported similar changes in the glass structure when adding Yb_2O_3 into the tellurite network due to the breakage of the $(\text{Te}_{\text{ax}}-\text{O})$ bonds of the TeO_4 units by Yb_2O_3 leading to the progressive formation of $\text{TeO}_3/\text{TeO}_{3+1}$ units.^[43] A similar trend was also observed in other works when adding La_2O_3 or Yb_2O_3 in tellurite glass.^[44,45] As the atomic packing factor is

Table 1. Thermal and physical properties of selected glasses.

Sample Code	T_g [°C] $\pm 3^\circ$ C	T_x [°C] $\pm 3^\circ$ C	T_p [°C] $\pm 3^\circ$ C	$\Delta T = T_x - T_g$ [°C] $\pm 6^\circ$ C	ρ [g cm ⁻³] ± 0.02 g cm ⁻³	V_m [cm ³ mol ⁻¹] ± 0.1 cm ³ mol ⁻¹
1.5Yb0.1Tm	353	481	515	128	5.56	26.47
2.5Yb0.05Tm	360	496	524	136	5.60	26.73
3.5Yb0.1Tm	372	534	550	162	5.67	26.85
4.5Yb0.1Tm	382	560	570	178	5.71	27.11

higher in the TeO₄ structural units than in the TeO₃ units, a decrease in the refractive index of the glasses when adding the RE is expected.^[46] The decrease is confirmed in Figure 1b. One should point out that all of the investigated glasses exhibit excellent thermal stability against crystallization as indicated by the large ΔT (>100 °C), making them great candidates for fiber drawing.^[47] The density of the glass was also found to be increasing with an increase in the RE content and the same happened to their molar volume, due to the higher molar mass of Yb₂O₃ (394.07 g mol⁻¹) and Tm₂O₃ (385.87 g mol⁻¹) compared to that of TeO₂ (159.60 g mol⁻¹), ZnO (81.39 g mol⁻¹), and BaO (153.33 g mol⁻¹).

The absorption spectra of the glasses (Figure 1c) clearly display the characteristic bands of Yb³⁺ in the 850–1050 nm range, corresponding to the ²F_{7/2} → ²F_{5/2} transition. The glasses, independently of their RE content, exhibit similar absorption cross-sections at 980 nm (1.03 × 10⁻²⁰ cm²), calculated using Equation (1), which aligns with the values reported for other Yb³⁺ doped tellurite-based glasses.^[48] The absorption band at 808 nm, associated with the ³H₆ → ³H₄ transition of Tm³⁺, is present but appears with low intensity due to the low Tm₂O₃ content in the glasses. All the glasses exhibit similar bandgaps independently of their RE content.

The upconversion spectra of the glasses were obtained using a 980 nm laser excitation. The upconversion spectrum of the 3.5Yb0.1Tm glass, taken as an example, is shown in Figure 2a. The spectrum exhibits the typical upconversion emission bands from the Tm³⁺ ions in the blue (≈ 475 nm) and the red regions (≈ 650 nm), corresponding to the ¹G₄ → ³H₆ and ¹G₄ → ³F₄ transitions, respectively; one should notice the absence of the emission bands at 360 nm (¹D₂ → ³H₆) and 450 nm (¹D₂ → ³F₄). No changes in the shape of the upconversion emission bands were observed when varying the RE concentration. As shown in

Figure 2b, increasing the concentration of Tm³⁺ and Yb³⁺ ions leads to an increase in the emission intensity at 475 nm, reaching a maximum when doping the glass with 2.5 mol% of Yb₂O₃ and 0.05 mol% of Tm₂O₃. The further increase in RE concentration decreases the intensity of the blue emission due to concentration quenching, likely caused by the reduced interionic distances between Tm³⁺-Tm³⁺, which enhance cross-relaxation interactions.^[49] The number of photons involved in the upconversion process in 3.5Yb0.1Tm glass was estimated from the slope of the logarithmic plot of upconversion emission intensity versus excitation power (Figure 2c) and was found to be similar for all the investigated samples. These slopes were found to be 2.41 and 2.37, respectively, indicating that the blue and red emissions are most likely due to three-photon absorption processes.^[49–52] The upconversion mechanism can, then, be described as follows: Yb³⁺ ions initially at the ²F_{7/2} ground state are excited to the ²F_{5/2} state via ground-state absorption under the 980 nm excitation. Yb³⁺ acts as a sensitizer and transfers the energy process from excited Yb³⁺ to Tm³⁺: ²F_{5/2} (Yb³⁺) + ³H₆ (Tm³⁺) → ²F_{7/2} (Yb³⁺) + ³H₅ (Tm³⁺). Then, the populated Tm³⁺ ions at ³H₅ excited state relaxes non-radiatively to the lower ³F₄ level. Next, either the same Yb³⁺ ion which absorbs a second 980 nm photon or another nearby Yb³⁺ ion being still in the ²F_{5/2} level, transfers its energy to the same Tm³⁺, and the mechanism in which the Tm³⁺ in the excited state ³F₄ absorbs a 980 nm photon is also possible. The Tm³⁺ reaches the ³F_{2,3} levels and then non-radiatively decays to the ³H₄ state. The Tm³⁺ ions at the ³H₄ state are further pumped into ¹G₄ state by energy transfer process as follows: ³H₄ (Tm³⁺) + ²F_{5/2} (Yb³⁺) → ¹G₄ (Tm³⁺) + ²F_{7/2} (Yb³⁺). The radiative transitions from the ¹G₄ state to lower energy levels result in the emission of visible light, including blue emissions ≈ 475 nm (¹G₄ → ³H₆), as well as in the red at 650 nm (¹G₄ → ³F₄).^[49–52]

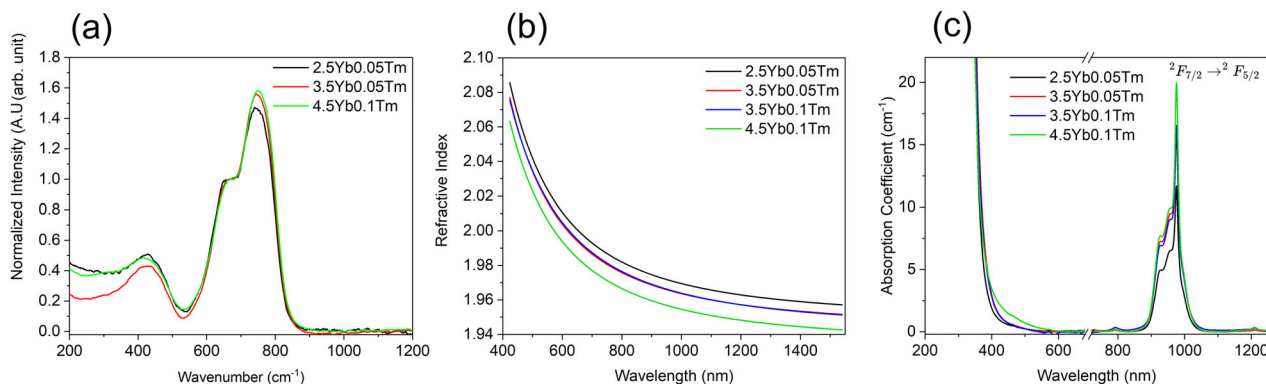


Figure 1. a) Raman spectra (785 nm excitation), b) refractive index dispersion, and c) absorption spectra of some selected xYb/Tm glasses.

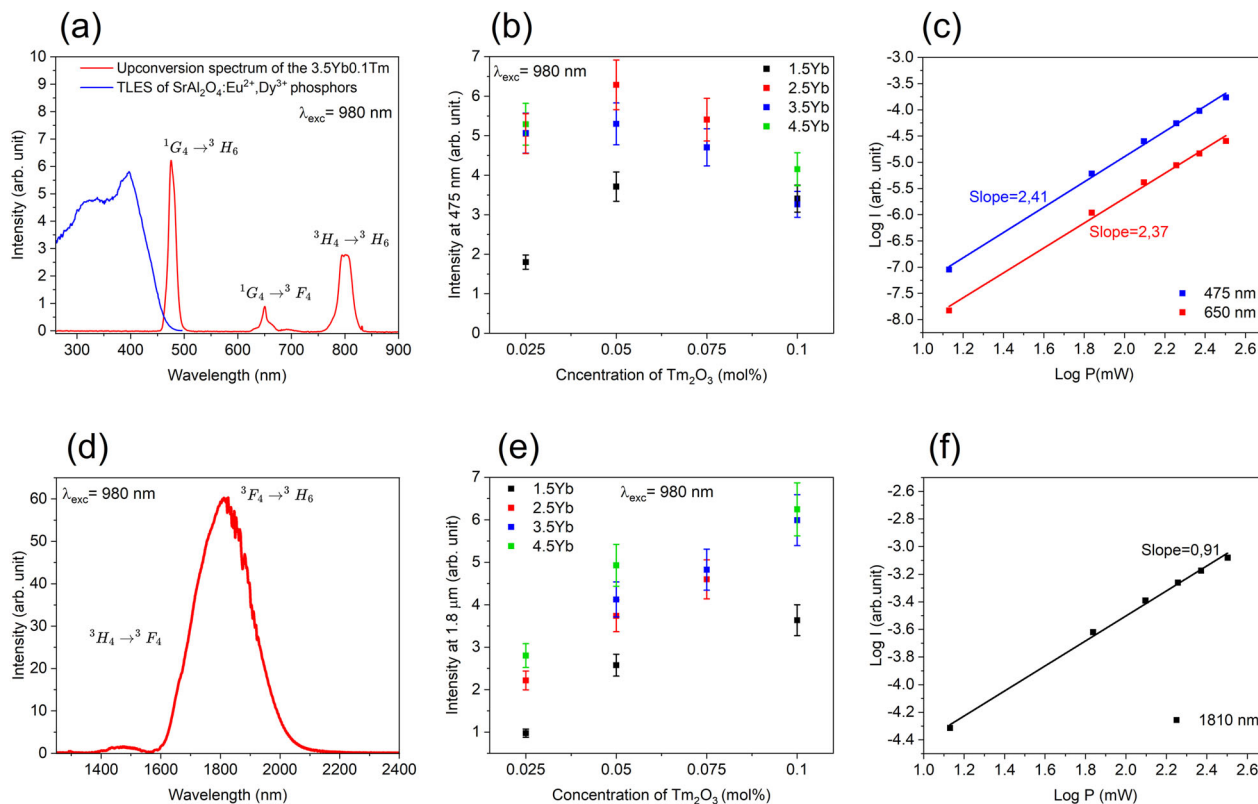


Figure 2. a) Upconversion spectrum of the 3.5Yb0.1Tm glass obtained using an excitation laser at 980 nm with a power of ≈ 300 mW and spot size ≈ 2 mm, together with the thermoluminescence excitation spectrum (TLES) of the SrAl₂O₄:Eu²⁺, Dy³⁺ phosphors, taken from ref. [58] b) blue upconversion intensity as a function of RE content, c) slopes on a log–log scale, which represent a power-law dependency on the blue and red upconversion process in the 3.5Yb0.1Tm glass. d) Emission spectrum of the 3.5Yb0.1Tm glass obtained using excitation laser at 980 nm with a power of ≈ 300 mW and spot size ≈ 2 mm, e) intensity of the emission at 1810 nm as a function of RE content, f) slope on a log–log scale, which represents a power-law dependency on the process of the emission at centered at 1810 nm in the 3.5Yb0.1Tm glass.

In contrast, the infrared emission spectrum (Figure 2d, measured for the 3.5Yb0.1Tm glass taken as an example) shows a broad band centered at 1810 nm, corresponding to the $^3F_4 \rightarrow ^3H_6$ transition of Tm³⁺ ions, and a less intense band at 1460 nm which can be related to the $^3H_4 \rightarrow ^3F_4$ transition of Tm³⁺. [53] As shown in Figure 2e, the intensity of the emission at 1800 nm is significantly enhanced with the addition of Yb₂O₃ and Tm₂O₃, reaching a maximum intensity when using 4.5 and 0.1 mol%, respectively. The changes in the doping concentration or the excitation power do not affect the shape of the emission spectrum of the glasses. The number of photons (*n*) was also calculated for the emission at 1810 nm and it is presented in Figure 2f and it gives a slope of ≈ 0.91 , indicating that the IR emission originates primarily from a single-photon absorption process.

The PeL SrAl₂O₄:Eu²⁺, Dy³⁺ phosphors were incorporated into the 2.5Yb0.05Tm glass, as this glass exhibits the strongest blue upconversion emission under 980 nm excitation. The phosphors were added to the glass melt prior to quenching.[54] Composites with varying PeL concentrations (0.25, 0.5, and 1 wt.%) were prepared. A picture of the composites in daylight and after stopping the UV irradiation is shown in Figure 3a. An increase in the PeL concentration leads to a loss in the transmittance of the composites due to scattering, which is expected due to the size of the PeL crystals (50–150 μm),[55] and the refractive index mismatch be-

tween the glass matrix (≈ 1.98) and the SrAl₂O₄:Eu²⁺, Dy³⁺ crystals (≈ 1.76)^[56,57] (Figure 3b). Dark coloration of the composite is also observed when increasing the PeL phosphors concentration, which might be due to the reaction between the PeL particles and the glass.[28] Nonetheless, all samples exhibit uniform green afterglow after being charged with UV light, with the intensity of the emission increasing with the SrAl₂O₄:Eu²⁺, Dy³⁺ content. The green afterglow observed from the tellurite composites confirms the phosphors' survival throughout the melting process. The PeL spectra of the investigated PeL containing composites measured after 5-min charging at 254 nm and the photoluminescence (PL) spectra under 365 nm excitation are shown in Figure 3c,d, respectively. The spectra exhibit luminescence characteristics which are typical of Eu²⁺ ions, originating from the $4f^65d^1 \rightarrow 4f^7$ transition, with a broad emission band centered around ≈ 520 nm. However, the luminescence intensity is notably affected by the PeL doping concentration; at low concentration, the emission intensity is relatively weak due to the low amount of Eu²⁺ luminescent centers available. The decay curves of the composites after being charged with 254 nm for 5 min are shown in Figure 3e. All composites exhibit green afterglow above the visibility threshold of 0.3 mcd m⁻² and last at least 40 min for the composite with 1 wt.% of PeL.

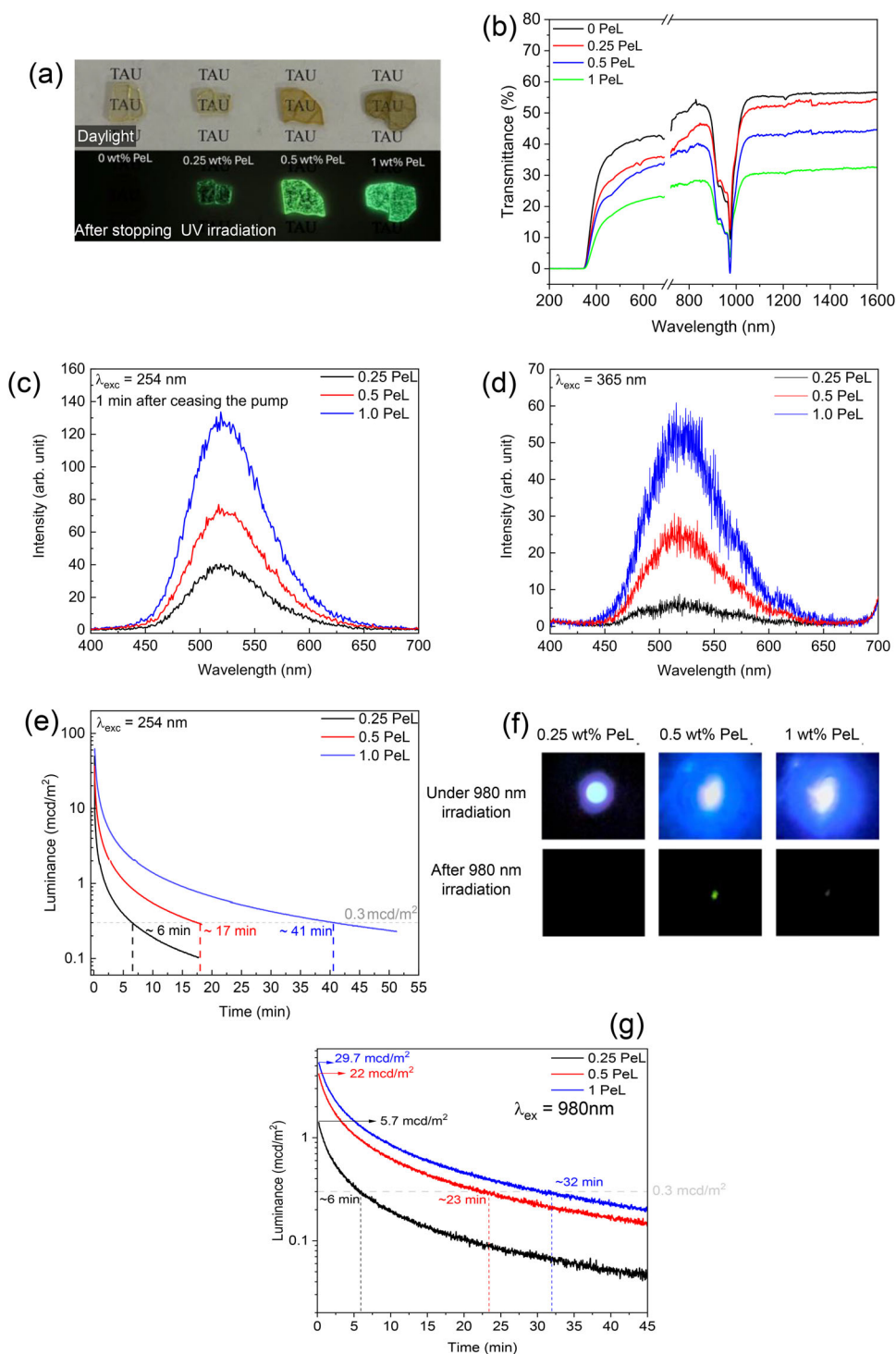


Figure 3. a) Picture of the composites with different SrAl₂O₄:Eu²⁺, Dy³⁺ content in the daylight and after stopping the UV charging for 5 min, b) transmittance spectra of the composites (thickness of the composites being $\approx 1 \text{ mm}$), c) PeL spectra after stopping the UV charging at 254 nm, d) PL under 365 nm excitation e) decay curve after stopping the UV charging at 254 nm, f) picture of the powder composites with different SrAl₂O₄:Eu²⁺, Dy³⁺ content under and after 980 nm irradiation for 30 min, and g) decay curve after stopping the NIR charging at 980 nm.

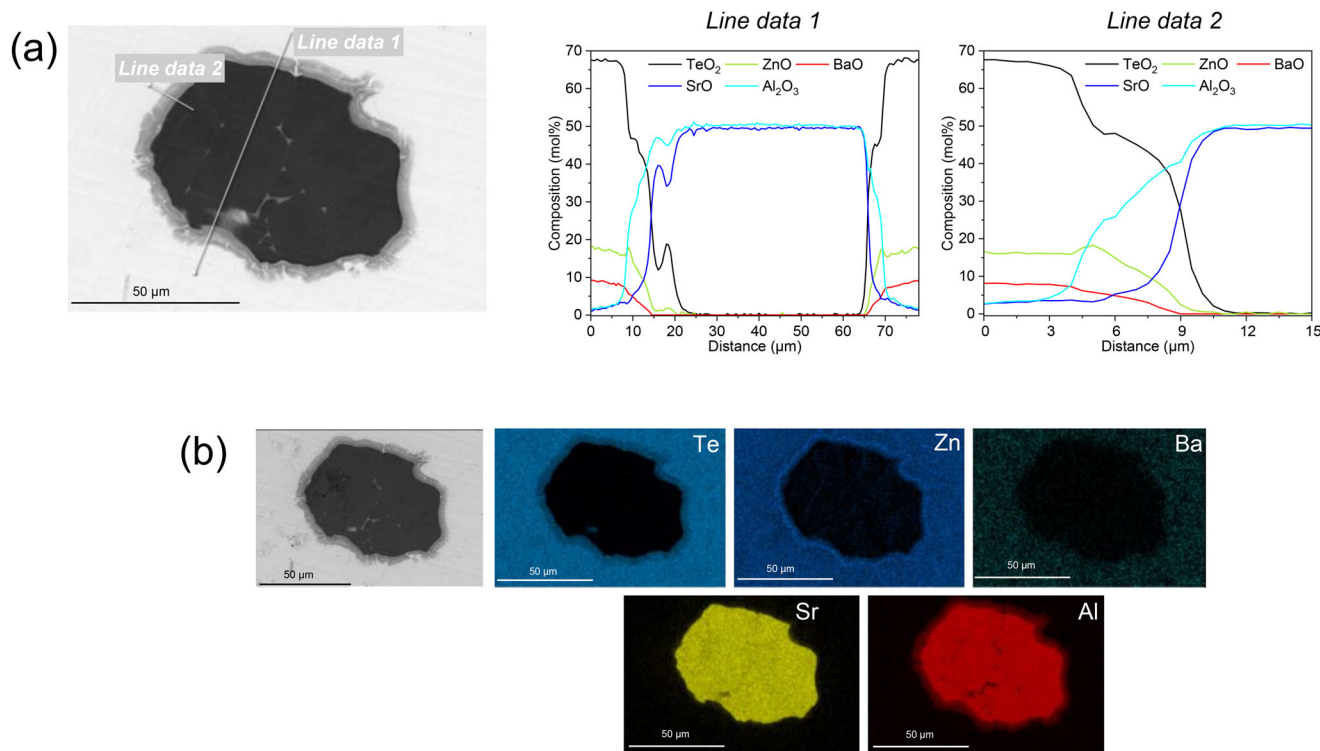


Figure 4. a) SEM Backscattered image and EDS line scans composition analysis across a PeL particle found at the surface of the composite prepared with 0.5 wt.% of PeL phosphors and b) Elemental mapping of a PeL particle found at the surface of the composite prepared with 0.5 wt.% of PeL phosphors.

More importantly, afterglow could be seen with naked eyes after charging for 30 min with 980 nm laser in the powder composites prepared with at least 0.5 wt.% of PeL phosphors, as shown in Figure 3f, suggesting that the blue upconversion from the 2.5Yb0.05Tm glass is strong enough to charge the phosphors in the composites, even though the blue emission at 475 nm has only limited overlap with the thermoluminescence excitation spectrum (TLES) of the $\text{SrAl}_2\text{O}_4:\text{Eu}^{2+}, \text{Dy}^{3+}$ phosphors as shown in Figure 2a.^[58] It is worth pointing out that trapped charges can be optically detrapped.^[59] It was found that trapped charges in $\text{SrAl}_2\text{O}_4:\text{Eu}^{2+}, \text{Dy}^{3+}$ feature an optical absorption spectrum from 500 nm to ≈ 950 nm, whereas at 980 nm there is no significant absorption.^[60] Using a 980 nm is thus essential in the present work, since at this wavelength the upconversion process can yield blue photons (inducing trapping in the PeL phosphor), while it does not optically release already trapped charges, or at least in a minimal way. Hence, irradiation with 980 nm leads to a net trapping effect. The increase in the content of the PeL phosphors increases the luminance as expected. After being charged with NIR, all composites exhibit green afterglow above the visibility threshold of 0.3 mcd/m² and last almost 30 min for the composite with 1 wt.% of PeL (Figure 3g).

Micro-scale investigation of the composites with embedded $\text{SrAl}_2\text{O}_4:\text{Eu}^{2+}, \text{Dy}^{3+}$ particles was performed. The SEM backscattered image and EDS line scans across a PeL particle found at the surface of the composite prepared with 0.5 wt.% of PeL phosphors confirm that the PeL particles survive the melting process (Figure 4a). According to the line scan, the PeL phosphors are expected to maintain their composition in their cen-

ters (Figure 4a,b). However, a layer enriched in Al_2O_3 and ZnO is suspected to form at the particle-glass interface which suggests partial decomposition of the PeL phosphors with the diffusion of Al from the PeL phosphors to the glass during the preparation of the composites. Similar partial decomposition of the PeL phosphors with a formation of Al-rich outer layer was reported when preparing PeL phosphate composites.^[55] It is worth noting that the composition of the tellurite glass aligns well with the theoretical values, within the measurement accuracy of ± 1.5 mol%.

Due to its promising combination of transparency and green afterglow, the composite prepared with 0.5 wt.% of $\text{SrAl}_2\text{O}_4:\text{Eu}^{2+}, \text{Dy}^{3+}$ was prepared as a crack-free preform with a 9 cm length and a 1 cm diameter. The preform was subsequently drawn into a fiber. Polymer coating was not applied upon drawing allowing the characterization of the composite fiber. The pictures of the preform and various fiber pieces in daylight and after UV charging are shown in Figure 5a. The preform exhibits homogeneous green afterglow suggesting homogeneous dispersion of the PeL particles in the glass rod. Green afterglow is also observed from the fibers suggesting that the PeL particle also survived the drawing process. The presence of the PeL particle in the composite fibers is further confirmed using SEM (image and elemental mapping of the fiber cross section (Figure 5b)). No elongation or breakup of the PeL particles in the fiber was observed. No other crystals were found in the fiber confirming the thermal stability of the 2.5Yb0.05Tm glass against crystallization during the drawing process. The PL and PeL emission bands measured from the fibers crushed into powder remained unchanged, indicating that the Eu^{2+} sites in the PeL phosphors are not significantly affected

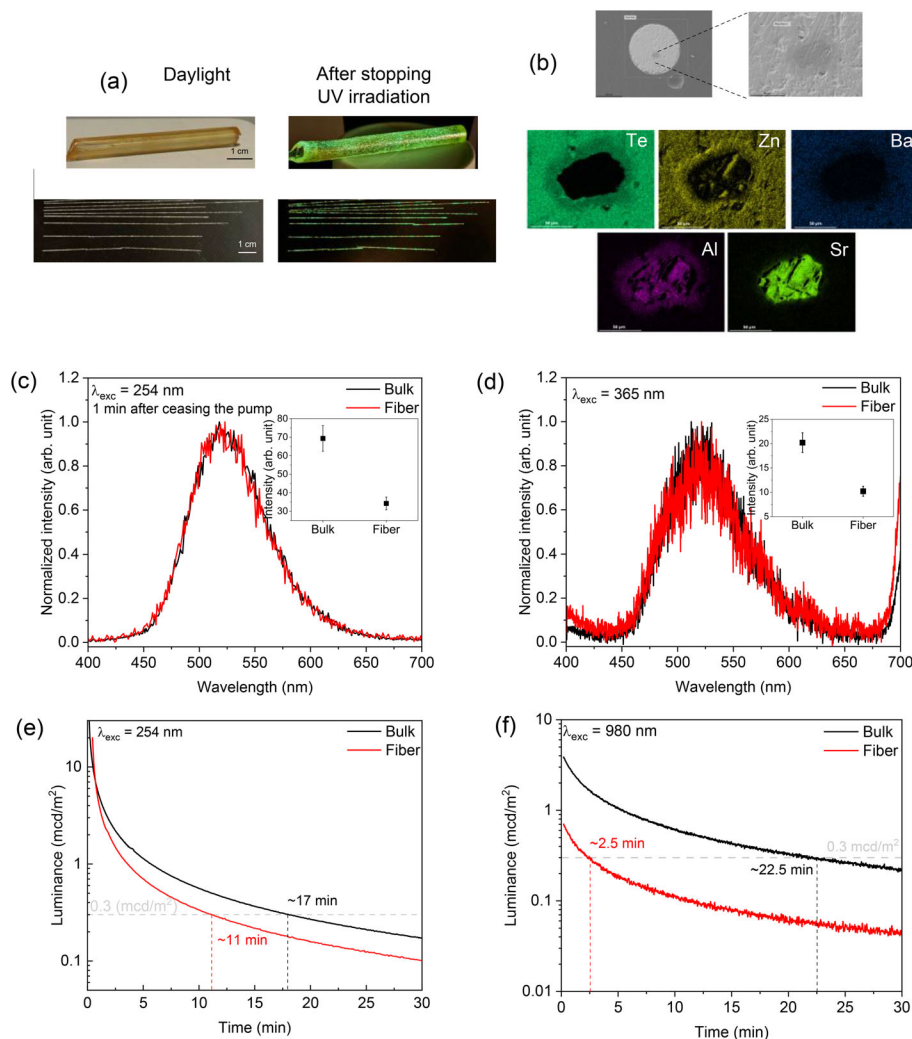


Figure 5. Pictures of a) the preform and pieces of fibers in daylight and after UV irradiation for 5 min. b) Backscattered image (BSE) of the composite fiber cross-section and in detail on the $\text{SrAl}_2\text{O}_4:\text{Eu}^{2+}, \text{Dy}^{3+}$ phosphor, c) Normalized PL emission spectra of the bulk and fiber during 365 nm excitation, inset is the peak intensities. d) Normalized afterglow spectra of the bulk and fiber after charging with UV for 5 min, inset is the peak intensities, e) bulk and fiber afterglow decay curve after charging with UV for 1 min and f) bulk and fiber afterglow decay curve after charging with NIR for 30 min.

by the drawing process (Figure 5c,d, respectively). However, under UV excitation at 365 nm and 254 nm, the photoluminescence (PL) and persistent luminescence (PeL) emission intensities in the fiber samples are $\approx 50\%$ lower than those observed in the bulk counterparts. Additionally, the visibility threshold of the green PeL afterglow decreases from 17 to 10 min post-drawing when excited with UV (Figure 5e), and from 22 to 2.5 min when excited with the NIR light (Figure 5f). As no alterations in the shape or intensity of the upconversion emission bands were observed after the drawing, the changes in the PeL properties can be related to the drawing process. Indeed, it is well known that a thermal treatment can play a significant role in altering the PeL and PL characteristics of the $\text{SrAl}_2\text{O}_4:\text{Eu}^{2+}, \text{Dy}^{3+}$ phosphors.^[29] Thermal processing affects the trap depth and density, thereby impacting the duration and intensity of the afterglow.^[61] Additionally, it can modify the PeL crystal structure, leading to variations in defect sites and luminescent centers, which in turn influence the efficiency of charge carrier trapping and recombination—key

elements for PeL.^[61] Therefore, the decrease in the PL and PeL properties suggests that the drawing process, despite being fast, affects the trapping and recombination mechanisms of charge carriers within the PeL particles, leading to shorter afterglow duration, not only after UV charging, but also after 980 nm charging as shown in Figure 5e,f.

The fiber absorption and guiding properties were studied. Due to the presence of PeL phosphors and various micro-cracks and defects in the as-drawn uncoated fibers, the scattering losses of the fibers are large. This can be observed in Figure 6a where the fiber glows bright under broad-spectrum light source excitation when photographed from the top. Nevertheless, the fiber retains guiding properties. The absorption and emission measurements were made by butt-coupling a multimode collection fiber to the output of the sample fiber and measuring the transmitted light. The absorption spectrum of the fiber, shown in Figure 6b exhibits a very strong absorption band at 980 nm typical of Yb^{3+} ions and another absorption band at 1400 nm characteristic of Tm^{3+} .

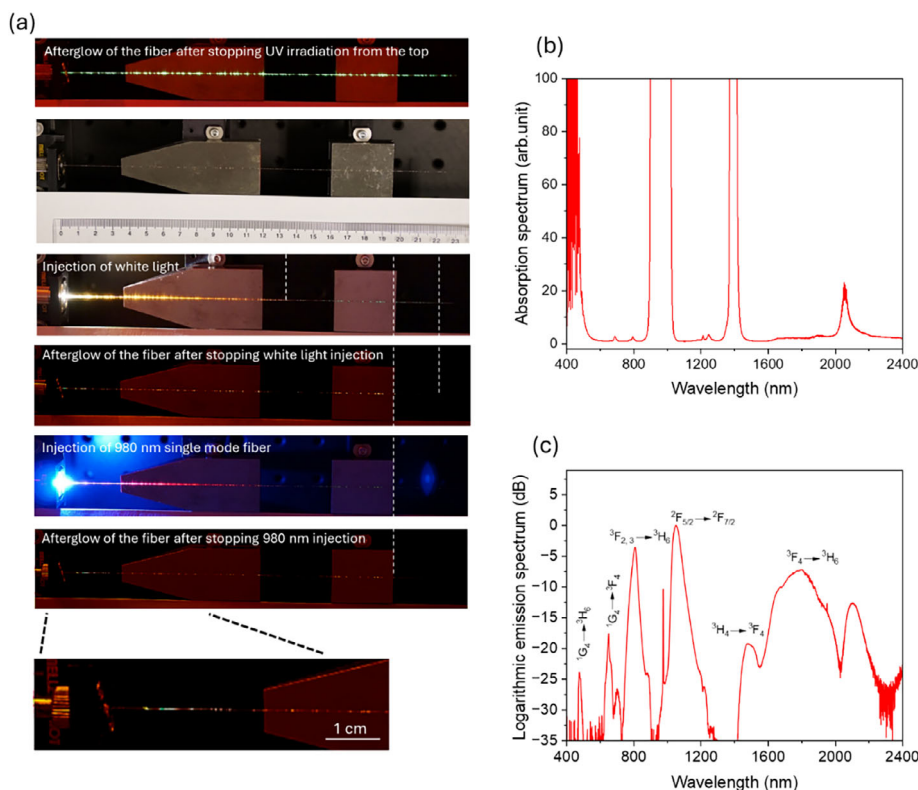


Figure 6. a) Pictures of the tellurite fiber (2.5Yb0.05Tm doped with 0.5 wt.% of $\text{SrAl}_2\text{O}_4\cdot\text{Eu}^{2+}$, Dy^{3+}) under different light conditions. b) Absorption spectrum of the fiber measured by a white light source. c) Emission spectrum of the fiber, the sharp peak at 980 nm is residual unabsorbed pump passing through the fiber.

Other weaker bands centered at 680 nm ($^3\text{H}_6 \rightarrow ^3\text{F}_{2,3}$), 793 nm ($^3\text{H}_6 \rightarrow ^3\text{H}_4$), 1240 nm ($^3\text{H}_6 \rightarrow ^3\text{H}_5$) belong also to Ti^{3+} ions as well as the very broad absorption starting at 1600 nm extending to 1800 nm ($^3\text{H}_6 \rightarrow ^3\text{F}_4$). The emission spectrum of the fiber upon 980 nm excitation (Figure 6c) exhibits the typical Ti^{3+} emission bands at 1470 and 1800 nm,^[62,63] as well as the upconverted Ti^{3+} emission bands at 470, 650, and 808 nm. Additionally, the strong broadband emission from the Yb^{3+} ions centered at 1030 nm can be seen.

Following 2 min of broad-spectrum light injection, the PeL phosphors exhibit a visible afterglow extending up to 13 cm from the light input in the case of the fiber presented in Figure 6a. Under 980 nm pumping, blue emission is observed in the first few centimeters of the fiber due to the high laser intensity, while red emission is seen few cm from the 980 nm pump. This behavior is attributed to the gradual reduction in excitation power along the fiber and the fact that blue upconversion involves more photons than red, thus requiring higher excitation power. After stopping the 980 nm excitation, afterglow can be also seen by naked eye up to 5 cm from the 980 nm input, demonstrating that the upconversion is strong enough to charge the PeL phosphors along the composite fiber.

3. Conclusion

In this study, we demonstrate the successful fabrication of composite fiber that exhibits green afterglow after the NIR charg-

ing. The fiber was drawn from a preform made of $\text{SrAl}_2\text{O}_4\cdot\text{Eu}^{2+}$, Dy^{3+} phosphors embedded in tellurite glass. The host glass was codoped with Yb^{3+} and Ti^{3+} to achieve the NIR-to-blue upconversion responsible for the charging of the PeL phosphors. First the Yb^{3+} , Ti^{3+} concentration was optimized to obtain the most efficient upconversion under the 980 nm laser excitation. Second, the composites were prepared by adding the PeL phosphors in the glass melt prior to quenching, allowing for the PeL phosphors to be homogeneously distributed in the glass matrix. The presence of the PeL phosphors in the composite bulks and fiber was confirmed not only from the green afterglow, but also using SEM/EDS. Despite the presence of PeL phosphors and defects on the surface of the uncoated fiber, light propagation was demonstrated, and the fiber exhibits visible green afterglow after NIR charging.

These results provide a promising foundation for the development of NIR-rechargeable PeL fibers for future use in advanced photonic applications requiring remote excitation, long-lasting luminescence, and integrated fiber-based design.

4. Experimental Section

Sample Fabrication—Glasses: Glasses with composition $(100-x-y)(70\text{TeO}_2 - 20\text{ZnO} - 10\text{BaO}) - x\text{Yb}_2\text{O}_3 - y\text{Ti}_2\text{O}_3$ where $x = 1.5, 2.5, 3.5$, and 4.5 mol% and $y = 0.025, 0.05, 0.075$, and 0.1 mol% (labeled as xY-byTi) were prepared using the melt-quenching method in an air atmosphere. The batches were prepared using the following raw materials TeO_2

(Sigma–Aldrich, 99.99%), ZnO (Sigma–Aldrich, 99.99%), BaO (Sigma–Aldrich, 99.99%), Yb₂O₃ (Sigma–Aldrich, 99.9%), and Tm₂O₃ (Sigma–Aldrich, 99.9%). The 10 g batches were melted in platinum crucible at 825–875 °C, depending on the glass composition, for 1 h. The molten glass was casted on a brass mold at room temperature followed by annealing at 250 °C for 5 h and then slowly cooled down to room temperature. Finally, the glasses were polished to perform the spectroscopic measurement.

Sample Fabrication—Composites: The composites were prepared by adding 0.25, 0.5, and 1 wt.% of the commercial SrAl₂O₄:Eu²⁺, Dy³⁺ PeL phosphors (from Realglow) into the molten 2.5Yb0.05Tm glass batch with the 68.22TeO₂-19.48ZnO-9.75BaO-2.5Yb₂O₃-0.05Tm₂O₃ composition (in mol%). The mixture was manually stirred prior to the quenching. After quenching, the composite bulks and preforms were then subjected to annealing at 250 °C for 5 h.

Sample fabrication—Composite Fiber: A cylindrical composite preform with a diameter of 1 cm and a length of 9 cm was prepared from the 2.5Yb0.05Tm glass prepared with 0.5 wt.% of PeL. The drawing process was performed at 490 °C under a helium flow of 2.5 L min⁻¹ to ensure an inert atmosphere. No coating was applied during the drawing process to facilitate the measurement of their properties. Few-meter fiber pieces with a diameter 400 μm were produced as in.^[22]

Characterization: The density of the bulk glasses was determined using the Archimedes method with ethanol as the immersion liquid. The results were obtained with an accuracy of ±0.02 g cm⁻³.

The thermal properties of the glasses were analyzed using differential scanning calorimetry (DSC) with a Netzsch 214 Polyma instrument. Samples were heated in platinum crucibles at a rate of 10 °C min⁻¹. The glass transition temperature (T_g) was determined from the inflection point of the endothermic peak, obtained via the first derivative of the DSC curve. The crystallization onset (T_c) and peak crystallization (T_p) temperatures were identified from the exothermic peak. All thermal properties are given with an accuracy of ±3 °C. Thermal stability against crystallization was evaluated as ΔT = T_x - T_g.

Raman spectra were acquired using a Renishaw inVia Qontor Raman microscope equipped with a cooled CCD camera. A 532 nm laser served as the excitation source.

A scanning electron microscope (SEM) (Crossbeam 540, Carl Zeiss, Oberkochen, Germany) equipped with an energy-dispersive spectroscopy (EDS) detector (X-MaxN 80, Oxford Instruments, Abingdon-on-Thames, UK) was used to obtain images and analyze the composition of the samples. To reduce charging effects, the samples were coated with a conductive carbon layer.

Absorption spectra were recorded using a UV–vis–NIR spectrophotometer (UV-3600 Plus, Shimadzu) over the wavelength range of 750–1200 nm with a measurement step of 0.5 nm. The absorption cross-section σ_{abs}(λ) was calculated with an accuracy of ±10% using the equation:

$$\sigma_{\text{abs}}(\lambda) = \frac{\ln(10) D(\lambda)}{NL} \quad (1)$$

where D(λ) represents the absorbance, N is the concentration of Yb³⁺ ions in the glass (ions/cm³), and L is the sample thickness.

The prism coupling technique with an Abbe refractometer (Model 2010/M, Metricon) was used to measure the refractive index of the investigated glasses at six different wavelengths: 443, 633, 825, 1061, 1312, and 1533 nm. Each wavelength was scanned multiple times, ensuring an accuracy of ±0.001.

The upconversion emission spectra of the (bulk) glasses and composites were measured using a Spectro 320-131 optical spectrum analyzer (Instrument Systems Optische Messtechnik GmbH), while the IR emission spectra (1600–2400 nm) were obtained using a monochromator coupled with an amplified MIR detector (PCI-4TE-4-1 × 1, preamplifier PIP-DC-200 M-F-M4, Vigo). The excitation was provided by a continuous-wave 980 nm monochromatic single-mode fiber-pigtailed laser diode (CM962UF76P-10R, Oclaro) with a power of ≈ 300 mW and spot size ≈ 2 mm. PL spectra were collected using a Varian Cary Eclipse Fluorescence Spectrophotometer equipped with a Hamamatsu R928 photomultiplier

tube (PMT) and 15 W xenon lamp. The emissions were measured by using the phosphorescence mode with 0.005 s total decay time and 365 nm excitation. The persistent luminescence (PeL) spectra were obtained before and after the composite drawing process using a Varian Cary Eclipse Fluorescence Spectrophotometer with a Hamamatsu R928 photomultiplier (PMT). A 4 W UV lamp (UVGL-25, λ_{exc}: 254 nm, 4 W) was used to excite the powder samples for 5 min, the emission spectra were measured 1 min after ceasing the irradiation. For PeL fading measurements, samples were irradiated for 1 min using a 254 nm hand-held UV lamp (UVGL-25). The PeL decay curves were done on crushed samples and recorded using a Hagner ERP-105 luminance meter coupled with a Hagner SD 27 detector, starting 5 s after excitation ceased, with luminance measured every 1s. The decay time was defined as the duration for PeL luminance to decrease to 0.3 mcd/m², with an accuracy determined by the noise level of individual measurements. For the PeL properties measurement, the sample was mounted in a dedicated sample holder, fixed to two orthogonal stepper motors. One moves left-right over 4 mm in a fast way (a few seconds), while in the other, perpendicular direction, the movement is a lot slower, but also over 4 mm. In this way, and considering the beam size, the beam covers most of the sample, with a diameter of 5 mm. Homogeneous afterglow was obtained from the samples with no visible damage observed.

All the measurements for the analysis of the spectroscopic properties of the glasses and composites were performed at room temperature. The glass and composite bulks were grinded into powder to allow the comparison of the emission intensity and obtain homogeneous results.

The emission spectra of the fiber were measured using a fiber-pigtailed 980 nm laser diode (Coherent). The output light was collected with a 200 μm multimode fiber and analyzed using an optical spectrum analyzer (OSA, ANDO AQ6317B). Transmittance measurements were performed using a fiber-pigtailed white light source (Anritsu MG922A). For PeL-fiber characterization, either a 980 nm fiber-coupled single-mode laser diode (CM96-500) or a fiber-coupled halogen white light source (Anritsu MG9224, 105 μm multimode fiber) was butt-coupled to the input end of the sample fiber. The output light at the distal end was collected using a 200 μm multimode fiber and analyzed with two separate OSAs (ANDO AQ6315B and Yokogawa AQ6375), covering a spectral range of 350–2400 nm.

Acknowledgements

This work was supported by the Research Council of Finland [Flagship Program, Photonics Research and Innovation PREIN-320165] and Business Finland (OFFULA project-2689). MN acknowledges the Weisell Foundation for funding.

Conflict of Interest

The authors declare no conflict of interest.

Data Availability Statement

The data that support the findings of this study are available from the corresponding author upon reasonable request.

Keywords

composite fiber, persistent luminescence, tellurite glass, upconversion

Received: July 13, 2025

Revised: September 12, 2025

Published online: October 26, 2025

- [1] P. Xiong, M. Peng, *J. Mater. Chem. C* **2019**, *7*, 8303.
- [2] C. Richard, B. Viana, *Light: Sci. Appl.* **2022**, *11*, 123.
- [3] J. Xu, S. Tanabe, *J. Lumin.* **2019**, *205*, 581.
- [4] L. C. V. Rodrigues, J. Hölsä, M. Lastusaari, M. C. F. C. Felinto, H. F. Brito, *J. Mater. Chem. C* **2014**, *2*, 1612.
- [5] T. Matsuzawa, Y. Aoki, N. Takeuchi, Y. Murayama, *J. Electrochem. Soc.* **1996**, *143*, 2670.
- [6] F. Liu, Y. Chen, Y. Liang, Z. Pan, *Opt. Lett.* **2016**, *41*, 954.
- [7] V. Castaing, A. D. Sontakke, A. J. Fernández-Carrion, C. Genevois, S. Tanabe, M. Allix, B. Viana, *Eur. J. Inorg. Chem.* **2017**, *2017*, 5114.
- [8] Y. Chen, L. Feng, L. Yanjie, W. Xianli, B. Jianqiang, W. Xiao-Jun, P. Zhengwei, *J. Mater. Chem. C* **2018**, *6*, 8003.
- [9] J. G. Valencia-López, N. F. Cano, B. J. Lopez-Flores, J. S. Ayala-Arenas, B. N. Silva-Carrera, J. Mosqueira-Yauri, *J. Lumin.* **2024**, *275*, 120807.
- [10] D. Poelman, D. Van Der Heggen, J. Du, E. Cosaert, P. F. Smet, *J. Appl. Phys.* **2020**, *128*, 240903.
- [11] J. J. Joos, K. Korthout, L. Amidani, P. Glatzel, D. Poelman, P. F. Smet, *Phys. Rev. Lett.* **2020**, *125*, 033001.
- [12] A. Kumar, D. M. A. Crista, A. Núñez-Montenegro, J. C. G. Esteves da Silva, S. K. Verma, *RSC Adv.* **2023**, *13*, 28676.
- [13] L. Wang, Z. Shang, M. Shi, P. Cao, B. Yang, J. Zou, *RSC Adv.* **2020**, *10*, 11418.
- [14] A. Lemiere, A. Szczodra, S. Vuori, B. Bondzior, T. W. Hawkins, J. Ballato, M. Lastusaari, J. Massera, L. Petit, *Mater. Res. Bull.* **2022**, *153*, 111899.
- [15] M.-H. Chan, Y.-C. Chang, *Anal. Bioanal. Chem.* **2024**, *416*, 3887.
- [16] N. Liu, X. Chen, X. Sun, X. Sun, J. Shi, *J. Nanobiotechnol.* **2021**, *19*, 113.
- [17] J. Zhang, Z. Wang, X. Huo, X. Meng, Y. Wang, H. Suo, P. Li, *Laser Photonics Rev.* **2023**, *18*, 2300751.
- [18] D. Przybylska, Grzyb T., A. Erdman, K. Olejnik, A. Szczeszak, *Sci. Rep.* **2022**, *12*, 19388.
- [19] X. Shen, A. Akbarzadeh, C. Shi, Z. Pang, Y. Jin, M. Ge, *J. Mater. Res. Technol.* **2021**, *13*, 1374.
- [20] M. Ge, X. Guo, Y. Yan, *Text. Res. J.* **2012**, *82*, 677.
- [21] X. Guo, K. Zhang, M. Ge, *Text. Res. J.* **2018**, *89*, 3601.
- [22] Z. Chen, Q. Cheng, H. Ke, Y. Li, Q. Wei, M. Ge, *Text. Res. J.* **2020**, *90*, 1783.
- [23] R. Barbosa, S. K. Gupta, B. B. Srivastava, A. Villarreal, H. De Leon, M. Peredo, S. Bose, K. Lozano, *J. Lumin.* **2020**, *231*, 117760.
- [24] L. Giordano, G. Cai, J. Seguin, J. Liu, C. Richard, L. C. V. Rodrigues, B. Viana, *Adv. Opt. Mater.* **2023**, *11*, 2201468.
- [25] P. Ge, K. Sun, H. Li, F. Yang, S. Ren, Y. Ding, *Optik* **2020**, *218*, 164944.
- [26] Y. Li, S. Zhou, Y. Li, K. Sharafudeen, Z. Ma, G. Dong, M. Peng, J. Qiu, *J. Mater. Chem. C* **2014**, *2*, 2657.
- [27] F. Liu, Y. Liang, Z. Pan, *Phys. Rev. Lett.* **2014**, *113*, 177401.
- [28] E. S. Magalhães, A. Sedda, B. Bondzior, S. Vuori, D. Van Der Heggen, P. F. Smet, M. Lastusaari, L. Petit, *Ceram. Int.* **2023**, *49*, 41150.
- [29] N. G. Arango, S. Vuori, H. Byron, D. Van Der Heggen, P. F. Smet, M. Lastusaari, L. Petit, *J. Alloys Compd.* **2022**, *927*, 167048.
- [30] Q. le Masne de Chermont, C. Chanéac, J. Seguin, F. Pellé, S. Maîtrejean, J. Jolivet, D. Gourier, M. Bessodes, D. Scherman, *Proc. Natl. Acad. Sci. USA* **2007**, *104*, 9266.
- [31] S. Tao, Y. Ping, F. Huang, Y. Hua, P. Qiao, Z. Xu, Y. Li, H. Ma, *Ceram. Int.* **2022**, *49*, 19606.
- [32] L. C. Barbosa, C. O. Filho, E. F. Chillce, In *Springer Series in Materials Science*, Springer, Berlin, New York **2017**, pp. 131–153.
- [33] J. Hrabovsky, F. Desevedavy, L. Strizik, G. Gadret, P. Kalenda, B. Frumarova, L. Benes, S. Slang, M. Veis, T. Wagner, F. Smektala, *J. Non-Cryst. Solids.* **2022**, *582*, 121445.
- [34] C. Strutynski, M. Evrard, A. L. Gendre, A. Maldonado, F. Désévéday, G. Gadret, J.-C. Jules, F. Smektala, *Materials* **2022**, *15*, 1177.
- [35] F. Désévéday, C. Strutynski, A. Lemièrre, P. Mathey, G. Gadret, J. Jules, B. Kibler, F. Smektala, *J. Am. Ceram. Soc.* **2020**, *103*, 4017.
- [36] A. Mori, *J. Ceram. Soc. Jpn.* **2008**, *116*, 1040.
- [37] M. Liao, C. Chaudhari, G. Qin, X. Yan, T. Suzuki, Y. Ohishi, *Opt. Express* **2009**, *17*, 12174.
- [38] C. Strutynski, F. Desevedavy, A. Lemièrre, J.-C. Jules, G. Gadret, T. Cardinal, F. Smektala, S. Danto, *Opt. Mater. Express* **2017**, *7*, 1503.
- [39] J. Žmojda, D. Dorosz, M. Kochanowicz, J. Dorosz, *Proceedings of SPIE, the International Society for Optical Engineering/Proceedings of SPIE 2011*, SPIE, Bellingham, WA **2011**.
- [40] D. Milanese, H. Gebavi, J. Lousteau, M. Ferraris, A. Schülzgen, L. Li, N. Peyghambarian, S. Taccheo, F. Auzel, *J. Non-Cryst. Solids.* **2010**, *356*, 2378.
- [41] G. Wang, S. Dai, J. Zhang, J. Yang, Z. Jiang, *J. Mater. Sci.* **2007**, *42*, 747.
- [42] A. Lemiere, B. Bondzior, I. Aromäki, L. Petit, *J. Am. Ceram. Soc.* **2022**, *105*, 7186.
- [43] N. Elkhoshkhany, S. Marzouk, M. El-Sherbiny, A. Ahmed, *J. Mater. Sci. Mater. Electron.* **2019**, *30*, 6963.
- [44] G. Gupta, S. Balaji, K. Biswas, A. Kalyandurg, *J. Am. Ceram. Soc.* **2018**, *101*, 3900.
- [45] M. Bardins, N. Vakula, L. Petit, *Scr. Mater.* **2024**, *255*, 116355.
- [46] W. A. Capanema, K. Yukimitu, J. C. S. Moraes, F. A. Santos, S. M. S. Figueiredo, V. C. S. Reynoso, O. A. Sakai, A. N. Medina, *Opt. Mater.* **2011**, *33*, 1569.
- [47] J. E. Shelby, *Introduction to Glass Science and Technology*, 2nd ed., Royal Society of Chemistry, Cambridge **2005**.
- [48] X. Feng, C. Qi, F. Lin, H. Hu, *J. Non-Cryst. Solids.* **1999**, *256–257*, 372.
- [49] D. K. Mohanty, V. K. Rai, Y. Dwivedi, *Spectrochim. Acta, Part A* **2012**, *89*, 264.
- [50] M. Liao, L. Wen, H. Zhao, Y. Fang, H. Sun, L. Hu, *Mater. Lett.* **2006**, *61*, 470.
- [51] Q. Zhang, L. Li, F. Liu, S. Li, X. Wei, W. Wang, H. Chen, Y. Pan, Y. Li, *J. Solid State Chem.* **2022**, *308*, 122927.
- [52] W. Wu, Y. Wang, L. Wu, H. Zhang, Z. Zhu, S. Ta, P. Zhang, S. Xu, B. A. Goodman, W. Deng, *ACS Photonics* **2024**, *11*, 2824.
- [53] B. Richards, S. Shen, A. Jha, Y. Tsang, D. Binks, *Opt. Express* **2007**, *15*, 6546.
- [54] V. Lahti, N. Ojha, S. Vuori, M. Lastusaari, Petit, L., *Mater. Chem. Phys.* **2021**, *274*, 125164.
- [55] N. Ojha, H. Nguyen, T. Laihininen, T. Salminen, M. Lastusaari, L. Petit, *Corros. Sci.* **2018**, *135*, 207.
- [56] C. F. Bohren, D. R. Huffman, *Absorption and Scattering of Light by Small Particles*, John Wiley & Sons, New Jersey **2008**.
- [57] J. Massera, M. Gaussiran, P. Gluchowski, M. Lastusaari, L. Hupa, L. Petit, *J. Eur. Ceram. Soc.* **2015**, *35*, 4051.
- [58] A. J. J. Bos, R. M. van Duijvenvoorde, E. van der Kolk, W. Drozdowski, P. Dorenbos, *J. Lumin.* **2011**, *131*, 1465.
- [59] D. Van der Heggen, J. J. Joos, A. Feng, V. Fritz, T. Delgado, N. Gartmann, B. Walfort, D. Rytz, H. Hagemann, D. Poelman, B. Viana, P. F. Smet, *Adv. Funct. Mater.* **2022**, *32*, 2208809.
- [60] D. Van der Heggen, J. J. Joos, D. Rytz, B. Viana, P. F. Smet, *J. Phys. Chem. Lett.* **2023**, *14*, 10151.
- [61] T.-H. Kim, H.-J. Hwang, J.-H. Kim, K.-T. Hwang, K.-S. Han, *J. Korean Cryst. Growth Cryst. Technol.* **2016**, *26*, 193.
- [62] B. Dussardier, W. Blanc, P. Peterka, *Tailoring of the Local Environment of Active Ions in Rare-Earth-and Transition-Metal-Doped Optical Fibres, and Potential Applications in Selected Topics on Optical Fiber Technology*, Intech, Rijeka **2012**, pp. 97–120.
- [63] S. D. Agger, J. H. Povlsen, *Opt. Express* **2006**, *14*, 50.